Photodissociation of *tert*-Butyl Iodide at 277 and 304 nm: Evidence for Direct and Indirect Dissociation in A-Band Photolysis of Alkyl Iodide

Yong Shin Kim, Wee Kyung Kang,*,† Dong-Chan Kim, and Kyung-Hoon Jung*

Center for Molecular Science and Department of Chemistry, Korea Advanced Institute of Science and Technology, Taeduck Science Town, Taejon 305-701, Korea

Received: February 14, 1997; In Final Form: May 12, 1997[⊗]

The photodissociation of t-C_4H_9I has been studied at 277 and 304 nm in a supersonic molecular beam. The fragments (I and t-C_4H_9 radical) are selectively ionized by resonance-enhanced multiphoton ionization and then projected onto a two-dimensional position-sensitive detector to obtain their translational energy and angular distributions. The energy distribution is found to consist of three components: one Maxwell−Boltzmann and two Gaussian distributions. Their anisotropy parameters range from 0.7 to 1.6 and display a parallel transition characteristic, where the greater the kinetic energy of the component, the stronger its anisotropy. From present and previous work, these three components are interpreted in terms of three independent reaction paths on an excited potential energy surface: (1) the prompt dissociation along the C−I stretching mode for the high-energy component, (2) the repulsive mode along the C−I stretching, coupled with some bending motions for the medium-energy component, and (3) the indirect dissociation, probably due to large contribution of the bending motions for the low-energy component. Relative quantum yields for $I(^2P_{3/2})$ at 277 and 304 nm have been determined and found to be 0.93 ± 0.03 and 0.92 ± 0.04, respectively. Experiments have shown that t-C_4H_9I has the highest curve-crossing probability from the $^3Q_0$ to $^1Q_1$ state among low-carbon alkyl iodides. The extensive vibrational coupling between two states in the proximity of a crossing point supports this interpretation.

I. Introduction

Photofragmentation of alkyl iodides in the A band has attracted substantial attention as a prototype model for the dissociation dynamics of polyatomic molecules over the last two decades.[1−15] Excitation of the A band, $\sigma^* \leftarrow$ N transition, in the 210−350 nm range, results in the breaking of a C−I bond to produce an alkyl radical in concert with either a spin-excited state $I(^2P_{1/2})$ atom (denoted I*) or a ground state $I(^2P_{3/2})$ atom (denoted I).[1,2] Three states from the σ^* configuration, $^3Q_1$, $^3Q_0$, and $^1Q_1$ states in Mulliken's notation, are dipole allowed from a ground state alkyl iodide.[16] The $^3Q_0$ state correlates with I* formation, with an associated dipole transition moment lying parallel to the C−I bond, while the $^3Q_1$ and $^1Q_1$ states correlate with I formation through perpendicular transitions.

Some extensive studies on the photodissociation of alkyl iodides have been reported for their first homologue and its derivatives, CH_3I,[2−7] CD_3I,[8,9] and CF_3I.[10−12] The study of the vibrational state distribution of the alkyl fragments, CX_3 (X = H, D, and F), has been a hot issue, since their dissociation dynamics can be relatively well confined within only an umbrella mode, ν_2, of the CX_3, under the simplified assumption of collinear pseudotriatomic dissociation due to prompt dissociation and because of their C_{3v} geometry. Although earlier experimental[2,17] and theoretical[18] studies support this picture for CH_3I, some recent experimental findings are quite controversial to this model. These are (1) the rotational excitation[5−7] around the axis perpendicular to the CH_3 top axis, (2) some excitations[5,7] of the ν_1 symmetric stretching mode, and (3) the beginning of the ν_2 bending motion after some elongation of the C−I bond.[3] These pieces of evidence represent the roles of other vibrational modes in addition to the ν_2 vibration in the dissociation dynamics and are well supported by theoretical calculations[19,20] using a multidimensional potential energy surface (PES). Mode-specific information on this multidimensional dissociation has been obtained from emission spectroscopy of dissociating alkyl iodides, *i.e.*, CH_3I, C_2H_5I, i-C_3H_7I, and t-C_4H_9I, within a short period, *ca.* 10 fs.[21,22] Their emission spectra show that bend−stretch combination bands exist in addition to the C−I stretch fundamental and its overtone. The bending motions relative to the stretch increase as the alkyl group becomes heavier and more branched. This suggests that a reaction coordinate of the photodissociation is a combination of the C−I stretch and bend modes, rather than just the stretch.

Photodissociation of t-C_4H_9I is a good choice for confirmation of this multidimensional character, since the molecule gives a large perturbation to simple C−I repulsive dissociation due to its tertiary structure and compares well with CH_3I because of its C_{3v} symmetry. According to magnetic circular dichroism (MCD) measurements, the A band of t-C_4H_9I is excited into a dominant $^3Q_0 \leftarrow$ N transition (centered near 270 nm) and two smaller contributions, $^3Q_1 \leftarrow$ N and $^1Q_1 \leftarrow$ N, located in the low- and high-energy wings, respectively.[23] The relative quantum yield for I production at 248 nm, 0.97,[24,25] can be explained by a high curve-crossing probability from the $^3Q_0$ state to the $^1Q_1$. Though its energy and spatial distributions still need to characterize the degree of orientation in oriented molecular beams,[26] they have not as yet been reported for the A-band photolysis of t-C_4H_9I.

In this paper, we report on the photodissociation dynamics of t-C_4H_9I at 277 and 304 nm, utilizing a state-selective photofragment imaging technique.[7,9,12] Translational energy and angular distributions are determined simultaneously for the I and t-C_4H_9 fragments. It is found that their energy distributions consist of one Maxwell−Boltzmann and two Gaussian components. These components have been interpreted in the light of the multidimensional PES. The relative quantum yields are

* Author to whom correspondence should be addressed.
† Present address: Division of Basic Science, Soongsil University, Seoul 176−763, Korea.
⊗ Abstract published in *Advance ACS Abstracts,* August 1, 1997.

S1089-5639(97)00574-4 CCC: $14.00

also obtained in order to clarify the dissociation channels at the two wavelengths.

II. Experiment

The experimental setup in this study has been described in detail elsewhere.[12,27] A mixture of 1% *t*-C_4H_9I (Aldrich Chemicals) seeded in He is injected into the reaction region using a molecular beam valve, pulsed at 10 Hz with a duration time of 200 μs/pulse. Photofragments from the ultraviolet photolysis of *t*-C_4H_9I are selectively ionized using resonance-enhanced multiphoton ionization (REMPI) within the same laser pulse. The laser light (typically 50 μJ/pulse, 0.1-cm^{-1} bandwidth, and 10-ns duration) is produced by doubling the output from a Nd:YAG-pumped dye laser. In the 277-nm region, a wavelength of 277.87 nm is used to selectively ionize the I atoms using a (2 + 1) REMPI process. In the 304-nm region, the I atoms are also selectively ionized at 304.67 nm. The frequency of the laser is scanned over 0.5 cm^{-1} in order to cover the entire Doppler profile of iodine atoms. The *t*-C_4H_9 fragment is also ionized efficiently in the 277- and 304-nm regions, presumably via a (1 + 1) REMPI process.[28] Two wavelengths of 277.70 and 304.40 nm are used to probe the *t*-C_4H_9 radical and are comparable to those of iodine atoms. In order to eliminate any interference by clusters, the time delay between the pulsed valve and the laser is controlled so as to photolyze only the leading edge of the molecular beam.

A time-of-flight mass spectrometer (TOFMS) is based on a design using single-stage acceleration. An extraction region of the TOFMS consists of a repeller plate with a 2-mm hole, through which the molecular beams pass to the reaction region, and a ground plate with 78% transmissive mesh (Buckbee-Mear, 200 lines/in.). The reaction zone is located 10 cm downstream from the valve. After ionization, the photofragment ions are accelerated along the molecular beam axis into the field-free region of the TOFMS and then projected onto a microchannel plate (MCP) backed by a phosphor screen (Galileo Electro-Optic Corp., 3040FM). A high-voltage pulse (−600 V in height and 1 μs in duration) is applied to the front plate of the MCP in order to increase the signal gain from a particular mass of interest. This process enables one to screen out the signals produced from the scattering of laser light and background ions with different masses. A transient screen image is recorded by using a CCD camera (Photometrics, CH250, 512 × 512) and is compiled for several thousand laser shots. Background noise is removed by subtracting the image collected with the laser tuned off-resonance under the same conditions.

III. Results

A. Relative Quantum Yields. Photoexcitation of *t*-C_4H_9I in the A band results in fission of the C−I bond. Two channels of the dissociation are represented by

$$t\text{-}C_4H_9I \rightarrow t\text{-}C_4H_9 + I^*/I \qquad (1)$$

The branching ratio of I* to I is proportional to the ion signal ratio by

$$\frac{N(I^*)}{N(I)} = k\frac{S(I^*)}{S(I)} \qquad (2)$$

where $S(i)$ refers the measured intensity of species i, $N(i)$ is the number of ith fragment atoms, and k is the proportionality constant. The k values are obtained from I_2 under the same experimental conditions, since its photodissociation is known to produce equal amounts of N(I) and N(I*) in the 277- and 304-nm regions.[29] Ion signals of the two channels are measured using the REMPI technique at 277 and 304 nm, and the branching ratio is calculated using eq 2. From the branching ratio, relative quantum yields of Φ(I) and Φ(I*) are determined from the relations

$$\Phi(I) = \frac{N(I)}{N(I^*) + N(I)} \quad \text{and} \quad \Phi(I^*) = 1 - \Phi(I) \qquad (3)$$

The Φ(I) are 0.93 ± 0.03 at 277 nm and 0.92 ± 0.04 at 304 nm, indicating a predominant production of the ground state iodine atoms at both wavelengths.

B. Ground State Iodine Atoms from *t*-C_4H_9I Photolysis. Figure 1 shows the raw images of an I atom at 277 and 304 nm. The 277-nm image in Figure 1a displays a cone shape, which is different from the typical polar-cap appearance of photofragment images of CH_3I[7] and CF_3I.[12] This difference may be interpreted in terms of the presence of an additional dissociation path with a low translational energy and weak anisotropy as well as the normal path of alkyl iodides with high kinetic energy and strong anisotropy. The 304-nm image in Figure 1b appears to be similar to that at 277 nm, which demonstrates that photoexcitation to excited states and subsequent dissociation dynamics are not greatly different at these two wavelengths.

A full three-dimensional (3-D) velocity distribution is reconstructed from the two-dimensional (2-D) velocity projection by using an inverse Abel transformation.[30] Due to the cylindrical symmetry of the velocity distribution, every planar slice containing the symmetry axis is equivalent and can be represented as a 2-D function of v_x and v_y, *i.e.*, the velocity perpendicular and parallel to the laser polarization, respectively. These contour maps, $P(v_x,v_y)$'s, are shown in Figure 2. Although there is the blurring effect resulting from the cylindrical overlapping geometry between the laser and molecular beams, the slow moving components are found to exist evidently.

By integrating the 3-D velocity distribution over all angles at each speed, we obtain the speed distribution $P(v)$. This speed distribution is readily transformed into a total center-of-mass translational energy distribution $P(E_t)$ using the equation

$$P(E_t) = P(v)\frac{dv}{dE_t} \qquad (4)$$

The dotted line in Figure 3 represents observed $P(E_t)$. Two kinetic energy components clearly appear in the $P(E_t)$: one is the sharply rising component near 0 kcal/mol, and the other is a broad distribution with a peak around 24 kcal/mol. From this distribution shape, it is reasonable to say that the former has a Maxwell−Boltzmann distribution and the latter a Gaussian. In practice, the two components are not sufficient to fit into the observed $P(E_t)$. Thus, the distribution function is assumed to consist of one Maxwell−Bolzmann distribution at low kinetic energy and two Gaussians at higher values. This function is expressed by the equation

$$P(E_t) = C_1\sqrt{E_t}\exp\left(-\frac{E_t}{kT}\right) + \sum_{i=2}^{3} C_i \exp\left\{-\left(\frac{E_t - E_i^\circ}{\Delta E_i}\right)^2\right\} \qquad (5)$$

where C_i is the coefficient for the ith term contribution, k the Boltzmann constant, T the temperature of the Boltzmann distribution, E_i° the peak energy of the Gaussian distribution, and ΔE_i the fwhm. The observed $P(E_t)$ is well demonstrated by the simulation using eq 5. The average translational energy, $\langle E_t \rangle$, of each component is calculated from the fitting function and is then corrected to compensate the blurring effect of the line source by the simulation study. The available energy, E_{avl},

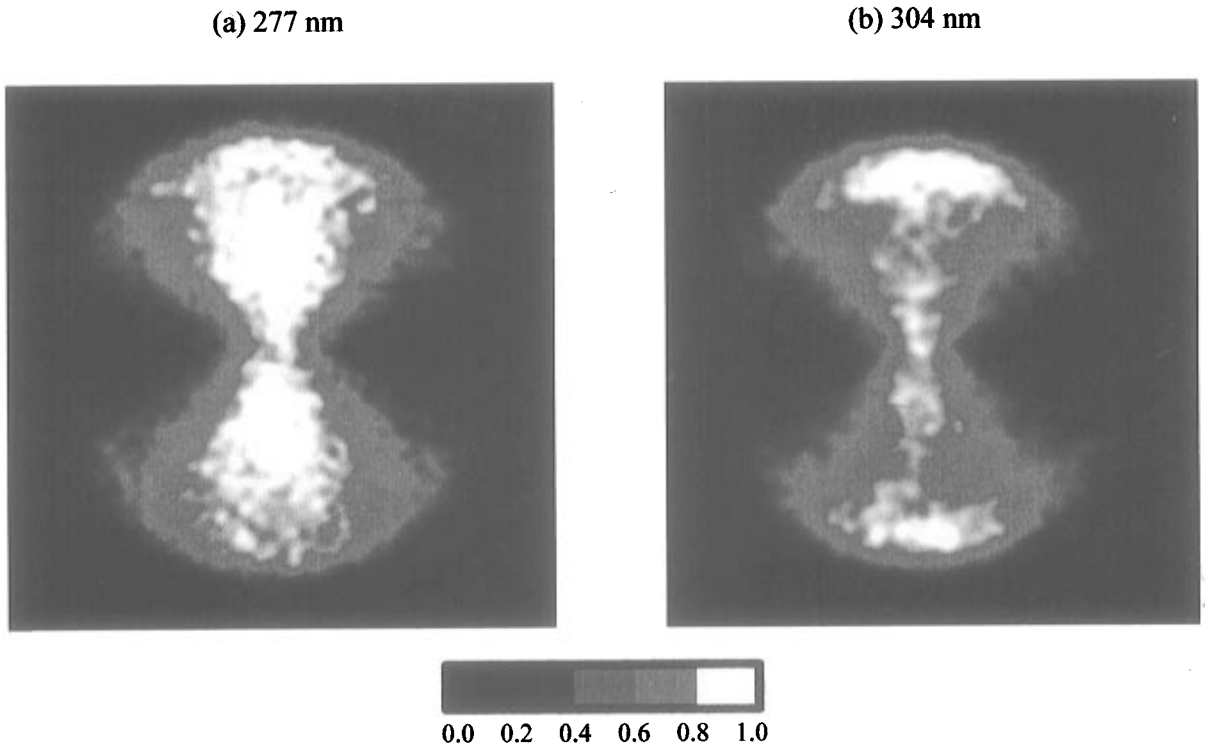

Figure 1. Raw images observed at two different wavelengths for the ground state of an iodine atom from *t*-C_4H_9I photolysis: (a) at 277.87 nm and (b) at 304.67 nm. The polarization vector of the laser is oriented vertically.

and the average internal energy of the *t*-C_4H_9 radical, $\langle E_{int} \rangle$, are determined from the energy conservation relationships

$$E_{avl} = E_{h\nu} - D_0^\circ + E_{int}^{P} \quad \text{and} \quad \langle E_{int} \rangle = E_{avl} - \langle E_t \rangle \quad (6)$$

where $E_{h\nu}$ is the photon energy, D_0° the dissociation energy of the C−I bond at 0 K, and E_{int}^{P} the internal energy of the parent molecule. The D_0° (51.0 kcal/mol) is obtained by subtracting the thermal energy[13] from the bond dissociation energy[31] at 298 K. The E_{int}^{P} is assumed to be zero because of the use of a supersonic molecular beam. The values of $\langle E_t \rangle$ and $\langle E_{int} \rangle / E_{avl}$ are listed in Table 1 together with the relative contribution of each component.

Angular distribution $P(\theta)$ is obtained by integrating the $P(v_x, v_y)$ over all speeds at constant angles, where $\theta = \tan^{-1}(v_x/v_y)$ and is the angle between the laser polarization and the recoil velocity of the fragment. The $P(\theta)$ for each component is extracted from above the half-maximum of each fitting function in the speed region and is fitted into the standard formula[32]

$$P(\theta) \propto [1 + \beta P_2(\cos \theta)] \quad (7)$$

where β is the anisotropy parameter, and $P_2(\cos \theta)$ the second-order Legendre polynomial. Angular distributions of the three components at 277 nm are displayed in Figure 4. The anisotropy parameters obtained are corrected to compensate the blurring of the line source and are listed in Table 1. It is found that the Gaussian distributions are much larger anisotropies than the Boltzmann and the high-E_t Gaussian is slightly larger than the low-E_t.

C. *tert*-Butyl Radical from *t*-C_4H_9I Photolysis. Images of *t*-C_4H_9 fragments are also observed at 277 and 304 nm in order to support the results obtained from I atoms. Translational energy distributions are obtained using the analytical method described above and are displayed in Figure 5. Since the quantum yields of I are larger than the value of 0.9, *t*-C_4H_9 fragments are mainly produced via the I formation channel, which provides the opportunity to cross-check the results of I

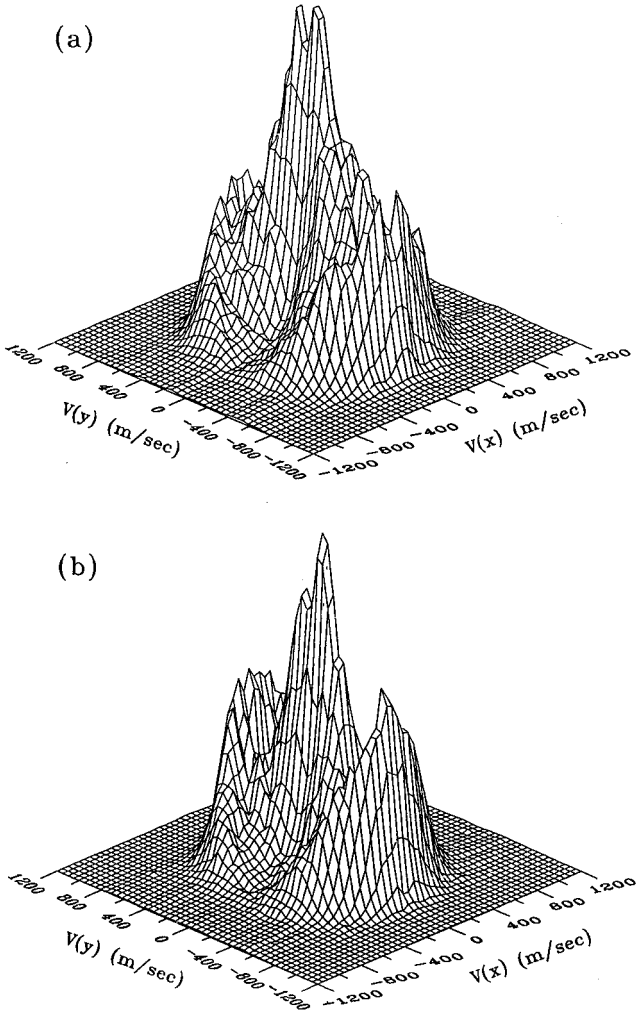

Figure 2. Product velocity contour maps for the I fragments produced by *t*-C_4H_9I photodissociation at (a) 277.87 and (b) 304.67 nm. The *x*- and *y*-axes correspond to velocity perpendicular and parallel to the laser polarization, respectively.

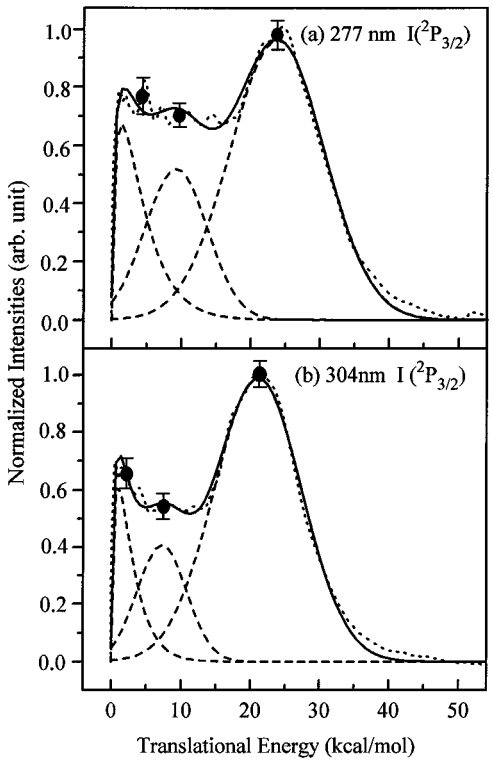

Figure 3. Total translational energy distribution, $P(E_t)$, obtained from the I fragments in *t*-C_4H_9I photodissociation at (a) 277 and (b) 304 nm. Dashed lines (---) show the best-fitting lines assuming one Boltzmann function for the low-energy component and two Gaussian functions at higher energy. The solid line (—) is a sum of the three simulated distributions and the dotted line (···) represents the experimental result. The vertical bars represent uncertainty limits at the average energies of the three components, estimated by the separate analysis of the upper and lower parts of the image.

TABLE 1: Energy Partitionings, Average Anisotropy Parameters, and Relative Contributions for the Three Components in the *t*-C_4H_9 + I($^2P_{3/2}$) Channel[a]

wavelength (nm)	$\langle E_t \rangle^b$	$\langle E_{int} \rangle / E_{avl}$	$\langle \beta \rangle^c$	relative contribution
277.87	4.2	0.92	0.8	0.15
	9.3	0.82	1.4	0.22
	24	0.54	1.5	0.63
304.67	2.8	0.93	0.7	0.11
	7.2	0.83	1.3	0.17
	21	0.51	1.6	0.72

[a] Energies are kcal/mol. [b] Average translational energy of each simulated function in Figure 3. [c] Average anisotropy parameter was determined at the region above the half-maximum of each fitting function.

atoms with that of *t*-C_4H_9 radicals on the basis of the momentum conservation law. The average translational energy and anisotropy parameter of each component are nearly the same in the two fragments, which implies that the three components in Figure 3 result from the dissociation channel of the I + *t*-C_4H_9 formation predominantly. However, the relative contributions of the three components disagree in the two cases. This discrepancy can be interpreted by the fact that the *t*-C_4H_9 fragments have a particular vibrational state distribution and resultant different MPI efficiency with variation of their translational energy at a given photon energy, while the detection efficiency of I atoms is constant throughout.

IV. Discussion

Relative quantum yields among possible reaction channels give valuable information about initial photoexcitations and the consequent dissociation dynamics. The relative quantum yield

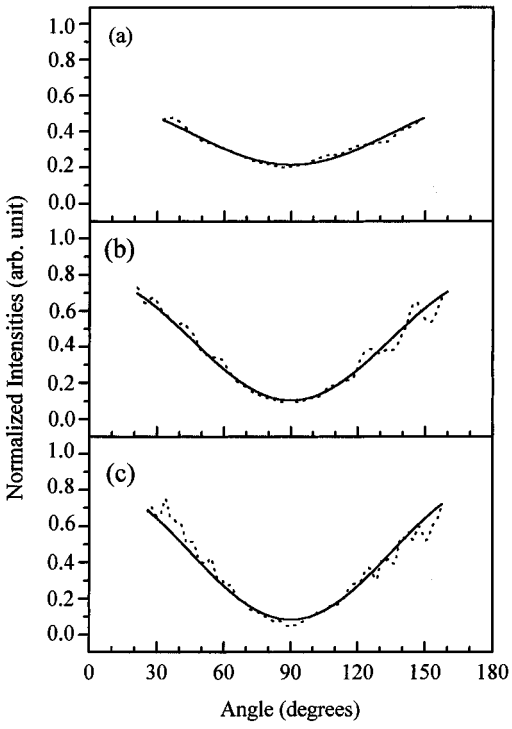

Figure 4. Angular distributions for the three components in the $P(E_t)$ of I photofragments at 277 nm; (a) Boltzmann, (b) low-E_t Gaussian, and (c) high-E_t Gaussian components of Figure 3a.

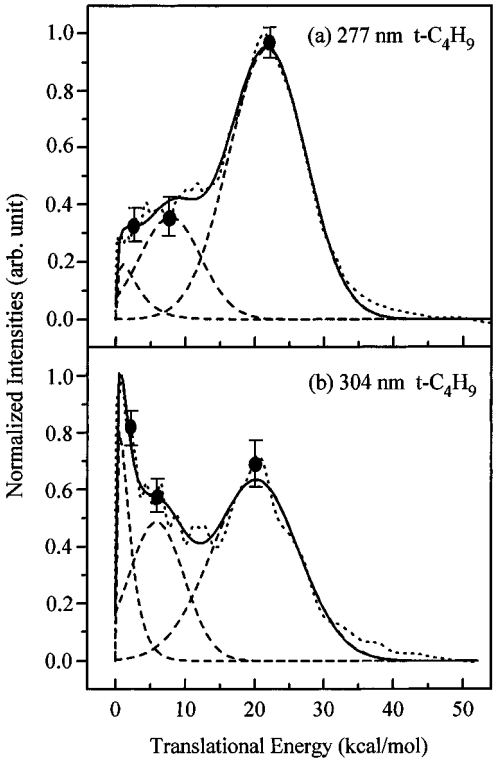

Figure 5. Total translational energy distribution, $P(E_t)$, obtained from the *t*-C_4H_9 fragment in *t*-C_4H_9I photodissociation at (a) 277 and (b) 304 nm. Dashed lines (---) show the best-fitting lines assuming one Boltzmann function for the low-energy component and two Gaussian functions for high energy. The solid line (—) is a sum of the three simulated distributions, and the dotted line (···) represents the experimental result. The vertical bars represent uncertainty limits at the average energies of the three components, estimated by the separate analysis of the upper and lower parts of the image.

of the I channel, $\Phi(I)$, has been obtained and found to be 0.93 at 277 nm. According to MCD,[23] the $^3Q_0$ and $^3Q_1$ states contribute only to the absorption cross section at 277 nm, where their contributions are 78 and 22%, respectively. Since the $^3Q_0$

and $^3Q_1$ states are diabatically related to the products of *t*-C_4H_9 + I* and *t*-C_4H_9 + I, the high Φ(I) should have originated from the initial transition to the $^3Q_1$ state. If this is correct, the angular distribution for I fragments must show the characteristic of perpendicular transition. The observed parallel angular distribution prevents this interpretation. The surface crossing is induced by nonadiabatic coupling between the excited $^3Q_0$ and $^1Q_1$ states in alkyl iodide. The high Φ(I) is therefore interpreted as a result of the $^3Q_0 \leftarrow$ N transitions, followed by the nonadiabatic curve crossing predominantly from the $^3Q_0$ to the $^1Q_1$ state. The high curve-crossing probability of *t*-C_4H_9I has been reported in earlier studies, in which the Φ(I) values are found to be 0.97 at 248 nm.[24,25]

The Φ(I) value at 304 nm has also been obtained and found to be 0.92. According to the MCD, the $^3Q_1$ state is formed substantially by perpendicular transition at 304 nm. Since the $^3Q_1$ does not intersect any state, one would expect that the relative quantum yields and angular distributions would reflect the dissociation dynamics on the $^3Q_1$ PES. In contrast to the prediction by the MCD, the excited PES has shown mostly the parallel transition to the $^3Q_0$ state in our angular distribution. A similar case has been found in the CF_3I system, in which the absorption at 308 nm, predicted to be exclusively the $^3Q_1 \leftarrow$ N transition by the MCD, has shown a substantial contribution from the $^3Q_0 \leftarrow$ N transition.[10] The high Φ(I) at 304 nm consequently suggests that the dissociation dynamics mainly follow the $^3Q_0$ transition and subsequently nonadiabatic transition to the $^1Q_1$ state as well as 277 nm.

The curve-crossing probabilities have been reported for various alkyl and substituted-alkyl iodides at 248 nm and have been rationalized by the one-dimensional Landau−Zener model with the impulsive energy disposal.[25] In this picture, the high curve-crossing probability of *t*-C_4H_9I has been explained with the change of the position of the crossing point due to the great electron donation to the α carbon: the crossing point is higher in energy or/and closer to the initial excitation point than other alkyl iodides. Since our high positive anisotropy parameter of I atoms at 304 nm shows the excitation to the $^3Q_0$ state followed by the curve crossing to the $^1Q_1$ state, the crossing point energy is lower than the 304-nm photon energy. If only the parallel transition to the $^3Q_0$ state occurs, the Φ(I) value is expected to increase in the above model by lowering the excitation energy into the crossing-point energy. However, this expected change has appeared neither in a literature value 0.97 at 248 nm nor in our quantum yields, 0.93 at 277 nm and 0.92 at 304 nm. This failure should be attributed to the fact that the dissociation of *t*-C_4H_9I is no longer described by the one-dimensional impulsive breaking of the C−I bond and the Landau−Zener theory. In fact, Person *et al.*[11] have experimentally observed this kind of failure from the branching ratio change in the CF_3I photodissociation with variation of temperature of the parent molecule. They have shown that an excitation of e-symmetry bending vibration, which distorts the molecules out of C_{3v} symmetry, induces the nonadiabatic transition due to the multidimensional nature of the coupling. The bending motions have been observed in the resonance Raman spectra of photodissociating alkyl iodides, and their contribution increases as the alkyl group becomes bulkier and branches about an α-carbon. The high nonadiabatic transition probability is therefore interpreted as an effect of an extensive excitation of bending modes and their couplings between the $^3Q_0$ and $^1Q_1$ states during the reaction. Even if we are not as yet to ready, the relative contributions of the three different dissociation channels and their nonadiabatic coupling characteristics must be taken into consideration in order to interpret the quantum yield variation according to the wavelength.

Energy partitioning in the A-band photolysis of alkyl iodides has been well understood in a direct dissociation framework and usually shows a Gaussian distribution in their translational energy distribution. In this work, we have found that two Gaussian and one Maxwell−Boltzmann functions are required to fit into the translational energy distributions $P(E_t)$. Godwin *et al.*[13] have reported that an fwhm of $P(E_t)$ of primary alkyl iodide is similar irrespective of radical size, while an fwhm for *i*-C_3H_7I is approximately twice as wide as that for *n*-C_3H_7I. From the above, it is expected that an fwhm for *t*-C_4H_9I should be broader than the primary and secondary iodides. Anomalously, the $P(E_t)$ of *t*-C_4H_9I has shown a Maxwell−Boltzmann component and two Gaussians. The Boltzmann is especially unusual considering the prompt dissociation of the C−I bond in alkyl iodide. No previous observations have reported that the energy partitioning of alkyl iodide has the characteristic of redistributing excess energy statistically. Three components can be identified from their angular and energy distributions.

The anisotropy parameters of the three components show stronger spatial anisotropy as the translational energy rises. The variation is due to mixed transition with parallel and perpendicular characters and the internal motions of an excited parent molecule. Although it exists, the effect of the mixed transition can be ignored due to the similar trend shown by variation according to translational energy at the two excitation energies and the two spin−orbit states of an iodine atom. The internal motions are vibrational and rotational motions on excited PES during dissociation. Up to date, there has been no simple model, even classically, to evaluate the effect of vibrational motions on the anisotropy parameter, because of its complexity. The dependence of β on rotational motion is classically expressed by the formula[34]

$$\beta = \beta_0 \frac{P_2(\cos\alpha) + \omega^2\tau^2 - 3\omega\tau \sin\alpha \cos\alpha}{1 + 4\omega^2\tau^2} \qquad (8)$$

where β_0 is the anisotropy parameter without rotational motion, $P_2(\cos\alpha)$ the second-order Legendre polynomial, ω the angular velocity, τ the lifetime of the parent, and α the deflection angle between the dissociation axis and the center-of-mass recoil velocity vector due to rotational motion. The angular velocity is determined from $I\omega^2 = kT$, where I is two large and equal moments of inertia of *t*-C_4H_9I and T is the rotational temperature estimated to be 50 K. If the anisotropy parameter results solely from a parallel transition with no vibrational motion, *i.e.*, $\beta_0 = 2$, the calculated upper limit of lifetimes for the three I channel components at 277 nm are 2.0, 0.90, and 0.85 ps in ascending order of kinetic energy, respectively. These indicate that the lifetime of the Boltzmann component is about 2 times longer than those of the Gaussians. Although this assumption is somewhat oversimplified since the bending motion in *t*-C_4H_9I photodissociation has been observed directly, it serves to give some insights into the three dissociation paths from their lifetimes. The two Gaussian components have shorter dissociation times than that of the Boltzmann; therefore they dissociate along a more repulsive coordinate.

The high-E_t Gaussian component, which contributed most, may be interpreted in terms of the classical impulsive model that has been used successfully for other alkyl iodide systems. In this model, a prompt dissociation assumption is made for along the C−I bond. Two models of this kind have been proposed by Riley and Wilson,[34] which represent two limiting cases: (1) the rigid radical limit, in which the alkyl radical is assumed to recoil as a rigid body so that only rotational excitation can occur, and (2) the soft radical limit, in which an α-carbon atom is assumed to be so weakly attached to the rest

of the alkyl radical that the C−I bond is broken quickly and then the kinetic energy of the α-carbon is redistributed into the translational and internal energy of the alkyl radical with conservation of energy and momentum. The $\langle E_{int}\rangle/E_{avl}$ values calculated using the rigid and soft models are 0 and 0.72, respectively. Our values of 0.54 and 0.51 at the two wavelengths for the high-E_t component suggest the soft radical limit. Consequently, the dynamics of the high-E_t component may be interpreted in terms of the direct dissociation along the C−I stretching and may be expected to result in the high vibrational excitations of t-C_4H_9 fragments due to C_{3v} geometry.

A low-E_t Gaussian component is also observed with its peak around 9 kcal/mol at 277 nm and 7 kcal/mol at 304 nm, respectively. Their $\langle E_{int}\rangle/E_{avl}$ values, 0.82 and 0.83, are larger than the predicted value of 0.72 from the soft radical model. Since the soft radical gives the maximum internal energy in the impulsive model, the low-E_t component cannot be explained by the impulsive framework. The high-E_t and low-E_t Gaussian components may be interpreted by the direct dissociation through the $^3Q_1$ state and curve-crossed dissociation from the $^3Q_0$ to $^1Q_1$ state. However, it is inconsistent with the parallel anisotropy for these two components and energy differences of the two Gaussian peaks, *ca.* 15 kcal/mol, which is too large to result from the two paths. This suggests a possibility that I atoms are produced from impurities containing an iodine atom and from other reactions in t-C_4H_9I except for the dissociation reaction producing I and t-C_4H_9. The possibility has also been excluded by observing two corresponding Gaussian components in $P(E_t)$ obtained from a t-C_4H_9 probe. Recent detailed experimental and theoretical reinvestigations of CH_3I photodissociation have provided strong evidence of some multidimensional character; that is, a dissociation coordinate is not due solely to the C−I stretching mode. Bend−stretch combination bands are also observed in the photodissociations of C_2H_5I, i-C_3H_7I and t-C_4H_9I using resonance Raman emission, as is the fact that the bending motions relative to the C−I stretch mode increased as the alkyl group become heavier and more branched.[22] The 266-nm Raman spectrum of t-C_4H_9I, with the strongest multidimensional character among the alkyl iodides, shows a nominal "bending" fundamental (ν_8) and a nominal CCH bend fundamental (ν_5) plus C−I stretch combination progressions, as well as the nominal C−I stretching fundamental (ν_7) and overtones. It is reasonable therefore to presume that the low-E_t Gaussian component results from a repulsive PES initially along the dissociation coordinate with the C−I stretch and the bend modes.

The Boltzmann component with the smallest translational energy may result from indirect dissociation on excited PES or unimolecular decay as a consequence of a radiationless transition to a hot ground state. To confirm the reaction route, the Boltzmann distribution is fitted into the equation

$$P(\mathrm{E_t}) \propto \left[\frac{E_{avl} - E_t}{E_{avl}}\right]^{s-1} \qquad (9)$$

where s is the number of effective vibrational modes in RRK formulation.[35] A value of $s \cong 15$ is obtained, which indicates a partial randomization of excess energy considering the total number of vibrational modes of t-C_4H_9I, 36. Since the unimolecular decay is generally accompanied by intramolecular vibrational relaxation, the partial randomization does not arise from the hot ground state. This is consistent with the observation that the Boltzmann component displays on the I* fragment image. Consequently, the Boltzmann distribution may be attributed to indirect dissociation along an initially bound reaction coordinate on excited PES, probably due to the large contribution of the bending motions.

Photon energy effects on dissociation dynamics give insight into the character of the multidimensional PES due to the change of the initially accessible regions. Contribution of the high-E_t Gaussian is higher at 304 than at 277 nm, which indicates that the dissociation dynamics has a greater multidimensional character as excess energy increases. The feature implies that the changes in the dissociation coordinates occur according to the excitation energy and that energy barriers may exist along the coordinates.

Acknowledgment. The authors gratefully acknowledge the Korea Research Foundation for the support (in part) of this research by the non-directed research fund, 1995−1998, and the Korea Science & Engineering Foundation by the Korea−Germany Joint Research Project, 1996−1999, and the Capital Equipment Grant, 1995−1997. One of authors (W.K.K.) also thanks the Korean Ministry of Education for the Research Grant, BSRI-96−3448.

References and Notes

(1) Riley, S. J.; Wilson, K. R. *Faraday Discuss. Chem. Soc.* **1972**, *53*, 132.
(2) Sparks, R. K.; Shobatake, K.; Carlson, L. R.; Lee, Y. T. *J. Chem. Phys.* **1981**, *75*, 3838.
(3) Lao, K. Q.; Person, M. D.; Xayariboun, P.; Butler, L. J. *J. Chem. Phys.* **1990**, *92*, 823.
(4) Suzuki, T.; Kanamori, H.; Hirota, E. *J. Chem. Phys.* **1991**, *94*, 6607.
(5) Zahedi, M.; Harrison, J. A.; Nibler, J. W. *J. Chem. Phys.* **1994**, *100*, 4043.
(6) Loo, R. O.; Haerri, H.-P.; Hall, G. E.; Houston, P. L. *J. Chem. Phys*. **1989**, *90*, 4222.
(7) Chandler, D. W.; Thoman, J. W., Jr.; Janssen, M. H. M.; Parker, D. H. *Chem. Phys. Lett.* **1989**, *156*, 151.
(8) Powis, I.; Black, J. F. *J. Phys. Chem.* **1989**, *93*, 2461.
(9) Chandler, D. W.; Janssen, M. H. M.; Stolte, S.; Strickland, R. N.; Thoman, J. W., Jr.; Parker, D. H. *J. Phys. Chem.* **1990**, *94*, 4839.
(10) (a) Felder, P. *Chem. Phys.* **1991**, *155*, 435. (b) Felder, P. *Chem. Phys. Lett.* **1992**, *197*, 425.
(11) Person, M. D.; Kash, P. W.; Butler, L. J. *J. Chem. Phys.* **1991**, *94*, 2557.
(12) Kim, Y. S.; Kang, W. K.; Jung, K.-H. *J. Chem. Phys.* **1996**, *105*, 551.
(13) Godwin, F. G.; Paterson, C.; Gorry, P. A. *Mol. Phys.* **1987**, *61*, 827.
(14) Zhu, Q.; Cao, J. R.; Wen, Y.; Zhang, J.; Zhong, X.; Huang, Y.; Fang, W.; Wu, X. *Chem. Phys. Lett.* **1988**, *144*, 486.
(15) Kang, W. K.; Jung, K. W.; Kim, D. C.; Jung, K.-H. *Chem. Phys*. **1995**, *196*, 363.
(16) Mulliken, R. S. *J. Chem. Phys.* **1940**, *8*, 382.
(17) Hermann, H. W.; Leone, S. R. *J. Chem. Phys.* **1982**, *76*, 4766.
(18) Shapiro, M.; Bersohn, R. *J. Chem. Phys*. **1980**, *73*, 3810.
(19) Amatatsu, Y.; Morokuma, K.; Yabushita, S. *J. Chem. Phys*. **1991**, *94*, 4858.
(20) Hammerich, A. D.; Manthe, U.; Kosloff, R.; Meyer, H.-D.; Cederbaum, L. S. *J. Chem. Phys.* **1994**, *101*, 5623.
(21) Hale, M. O.; Galica, G. E.; Glogover, S. G.; Kinsey, J. L. *J. Phys. Chem.* **1986**, *90***,** 4997.
(22) Phillips, D. L.; Lawrence, B. A.; Valentini, J. J. *J. Phys. Chem.* **1991**, *95*, 9085.
(23) Gedanken, A. *Chem. Phys. Lett.* **1987**, *137*, 462.
(24) Brewer, P.; Das, P.; Ondrey, G.; Bersohn, R. *J. Chem. Phys.* **1983**, *79*, 720.
(25) Godwin, F. G.; Gorry, P. A.; Hughes, P. M.; Raybone, D.; Watkinson, T. M.; Whitehead, J. C. *Chem Phys. Lett.* **1987**, *135*, 163.
(26) Xu, Q.-X.; Jung, K.-H.; Bernstein, R. B. *J. Chem. Phys.* **1988**, *89*, 2099.
(27) Kang, W. K.; Kim, Y. S.; Jung, K.-H. *Chem. Phys. Lett.* **1995**, *224*, 183.
(28) Wendt, H. R.; Hunziker, H. E. *J. Chem. Phys.* **1984**, *81*, 717.
(29) Clear, R. D.; Wilson, K. R. *J. Mol. Spectrosc.* **1973**, *47*, 39.
(30) Candel, S. M. *IEEE Trans. Acoust., Speech, Signal Process.* **1981**, *29*, 963.
(31) Cox, J. D.; Pilcher, G. *Thermochemistry of Organic and Organometallic Compounds*; Academic: New York, 1970.
(32) Zare, R. N. *Mol. Photochem.* **1972**, *4*, 1.
(33) Tadjeddine, M.; Flament, J. P.; Teichteil, C. *Chem. Phys.* **1987**, *118*, 45.
(34) Busch, G. E.; Wilson, K. R. *J. Chem. Phys.* **1972**, *56*, 3638.
(35) Marcus, R. A. *J. Chem. Phys.* **1975**, *62*, 1372.